

**Cu₂ZnSnS₄ (CZTS) THIN FILM GROWN BY
ELECTROCHEMICAL DEPOSITION FOR SOLAR CELL**

By

ELMOIZ MARGHNI MKAWI MRZOG

**Thesis submitted in fulfillment of the requirements
for the degree of Doctor of Philosophy**

March 2015

DEDICATION

To my parents: Thank you for teaching me to believe in myself, while always pushing me to do better. Your advice has helped me to make both the easy and hard decisions, and your support has given me the confidence to follow through.

To my beloved wife and kids: Who suffered and sacrificed a lot during my absence from Sudan. Thank you for believing in me, and for allowing me to further my studies.

Please do not ever doubt my dedication and love for you.

With respect

ACKNOWLEDGMENTS

All praise and thanks to Allah

I would like to acknowledge many people for their inspiration, mentoring, encouragement, and support. Without their invaluable help, I could not imagine how I would have completed my PhD. First of all, I owe the deepest gratitude to my advisor Professor Kamarulazizi Ibrahim for his encouragement, guidance, and support during the course of this dissertation research. In addition to his memorable stories delivered in our meetings, his enthusiasm and vision for the research have assisted and directed me to finish this PhD.

Along with this, a huge “thank you” goes to my co-supervisor Dr. Abd alsalam Mohammed for guidance through research challenges and the growth of the project. I am also very grateful to Universiti Sains Malaysia for providing financial support for my research and for giving me the chance to be a graduate assistant. I would like to thank all the staff from the School of Physics, Universiti Sains Malaysia, for providing a friendly environment in which I was able to conduct my project smoothly. I would like to thank the technicians of our School, especially the staff in the Nano Optoelectronics Research Laboratory, for their technical support and valuable contribution to my work. My thanks also go to the School of Chemistry at USM for providing me with the opportunity to use their laboratories and equipment.

Lastly, but by no means least, I would like to acknowledge my parents, my wife, and all my dear brothers and sisters in the Lord.

E.M.MKAWI

TABLE OF CONTENTS

	Page
DEDICATION	ii
ACKNOWLEDGEMENTS	iii
TABLE OF CONTENTS	iv
LIST OF TABLES	xiv
LIST OF FIGURES	xvi
LIST OF SYMBOLS	xiii
LIST OF MAJOR ABBREVIATION	xxvi
LIST OF PUBLICATIONS	xxiv
ABSTRAK	xxxi
ABSTRACT	xxiii
CHAPTER 1 : INTRODUCTION	1
1.1 The Energy Problem	1
1.2 Solar Energy	2
1.3 Thin Film Photovoltaics	3
1.4 Thin Film Photovoltaic Materials	5
1.5 Research Objectives	8
1.6 Originality of The Research Work	9
1.7 Outline of The Thesis	10
CHAPTER 2 : LITERATURE REVIEW	11
2.1 Introduction	11
2.2 Evolution of CZTS Thin Film Solar Cell Efficiency	11

2.3.	CZTS Thin Film Deposition Techniques	12
2.3.1	Vacuum-Based Techniques	12
2.3.1.1	Sputtering Techniques	13
2.3.1.2	Evaporation	14
2.3.1.3	Pulsed Laser Deposition Technique	16
2.3.2	Solution-Based Techniques	16
2.3.2.1	Precursor-Ink Based Approach	17
2.3.2.2	Spray Pyrolysis	18
2.3.2.3	Electrochemical Deposition technique	19
	CHAPTER 3 : THEORETICAL BACKGROUND	22
3.1	Introduction	22
3.2	Characteristics of $\text{Cu}_2\text{SnZnS}_4$ Thin Film	22
3.2.1	Structural Properties	23
3.2.1.1	Secondary Phases	25
3.2.2	Electrical properties	30
3.2.3	Optical Properties	31
3.2.4	Intrinsic Defects	32
3.2.5	Sulfurization	34
3.2.6	Introduction to CZTS Solar Cells	36
3.2.6.1	Effect of secondary phases on CZTS absorber layer and solar cells	39
3.2.7	Challenges in CZTS Fabrication Related to This Work	40
3.3	Fundamentals of Electrochemical Deposition	41
3.3.1	Introduction	41

3.3.2	Advantages of Electrochemical Deposition	42
3.3.3	Issues in Electrochemical Deposition of Semiconductors	42
3.3.4	Basic Principles of Electrochemical Deposition	43
3.3.5	The Three-Electrode Cell	46
3.3.6	Cyclic Voltammetry (CV)	47
3.3.7	Factors Governing Electrochemical Deposition	50
3.4	Basics of Solar Cells	50
3.4.1	p–n Junction Semiconductor	50
3.4.2	Performance Parameters of A Solar Cell	54
3.4.2.1	Short Circuit Current (I_{sc})	56
3.4.2.2	Open Circuit Voltage (V_{oc})	57
3.4.2.3	Fill Factor (FF)	57
3.4.2.4	Efficiency (η)	58
3.4.3	Diode Parameters of A Solar Cell	59
3.4.3.1	Series Resistance (R_s)	59
3.4.3.2	Shunt resistance (R_{sh})	60
	CHAPTER 4: EXPERIMENTAL PROCEDURES	63
4.1	Introduction	63
4.2	Soda Lime Glass Substrate Preparations	63
4.3	Molybdenum Back Contact	64
4.4	Methods of Fabricated of CZT Precursor and CZTS Nanocrystals	64
4.4.1	Electrochemical Deposition Cell	64
4.4.2	Rotary Evaporator and Three-Necked Flask	65

4.4.3	A centrifuge System	66
4.5	Sulfurization Process	67
4.6	Preparation of Electrolytes and Cyclic Voltammetry Setup	68
4.6.1	Growth of CZTS Thin Films Using Different Triangle Wave Pulse Time	68
4.6.2	Growth of CZTS Thin Films Using Different Complexing Agent	69
4.6.3	Growth of CZTS Thin Films Using Different Precursor Salts	69
4.6.4	Growth of CZTS Thin Films Using Different Stacking Order	70
4.6.5	Growth of CZTS Thin Films Using Different Substrate Temperature	70
4.6.6	Growth of CZTS Thin Films Using Different Sulfurization Temperature	71
4.6.7	Preparation of $\text{Cu}_2\text{ZnSnS}_4$ Nanocrystals Using Different Solvent Solution	71
4.6.8	Preparation of $\text{Cu}_2\text{ZnSnS}_4$ Nanocrystals Using Different Rotation Rates	72
4.7	The Relationship Between Applied Potential and Total Deposition Time	72
4.8	Fabrication of CZTS Devices	74
4.9	Coating Equipment	75
4.9.1	Metal Contacts Evaporation	75
4.9.2	Radio Frequency (RF) Sputtering System	76
4.10	Material Characterization Methods	77
4.10.1	X-ray Diffraction	78
4.10.2	Raman Spectroscopy	80

4.10.3	Field-Emission Scanning Electron Microscopy and Energy Dispersive Spectroscopy	81
4.10.4	Optical Reflectometer	82
4.10.5	Hall Effect	83
4.10.6	Ultraviolet–Visible Spectroscopy	86
4.10.7	Transmission Electron Microscopy	87
4.10.8	Characterization of Solar Cell Device	98
CHAPTER 5 : RESULTS AND DISCUSSION: CZTS Synthesis		90
5.1	Introduction	90
5.2	Influence of Triangle Wave Pulse on The Properties of $\text{Cu}_2\text{ZnSnS}_4$ Thin Films Prepared by Single Step Electrochemical deposition	90
5.2.1	Cyclic Voltammetry of CZT Precursors	91
5.2.2	XRD Analysis of CZTS Films	92
5.2.3	Raman Analysis of CZTS Films Deposited Under Different Triangle Wave Times	94
5.2.4	Surface Morphology of CZTS Films	96
5.2.5	Cross-Sectional Images of The Annealed CZTS (T_{300}) Thin Film	97
5.2.6	Compositional Analysis of The Precursor Film	98
5.2.7	Elemental Maps of A Field Of A CZTS Solar Cell Device	101
5.2.8	Optical Properties of The CZTS Thin Films	101
5.2.9	Properties of CZTS thin-film solar cells	103
5.3	Effect Of Complexing Agents On The Electrodeposition of Cu-Zn-Sn Metal Precursors and Corresponding $\text{Cu}_2\text{ZnSnS}_4$ -Based Solar Cells	106
5.3.1	Cyclic Voltammetry of CZT Precursors	107

5.3.2	XRD Peaks of CZTS Thin Films Prepared With and Without Complexing Agent	109
5.3.3	Raman Spectroscopy Of Samples Electrodeposited Using Different Complexing Agents	111
5.3.4	Chemical Compositions of The CZTS Thin Films	112
5.3.5	Surface Morphology of The CZTS Samples	114
5.3.6	Optical Properties of The Annealed CZTS Thin Films	115
5.3.7	Electrical properties of CZTS thin films	117
5.3.8	Cross-Sectional FESEM Image Of A CZTS Prepared Using Citrate	118
5.3.9	Device Efficiency of CZTS Solar Cells	119
5.4	Influence Of Precursor Salts On The Properties Of Electrochemical Deposition Of Cu-Zn-Sn Metal Precursors And Corresponding $\text{Cu}_2\text{ZnSnS}_4$ -Based Solar Cells	120
5.4.1	Cyclic Voltammetry (CV) Measurements	121
5.4.2	XRD Patterns of The CZTS Thin Films Prepared Using Different Salt Precursors	123
5.4.3	Raman Spectroscopy of The CZTS Thin Films	125
5.4.4	Morphology of CZTS Films Prepared Using Different Salt Precursors	126
5.4.5	Elemental maps of a field of a CZTS thin film	127
5.4.6	Cross-Sectional FESEM Image of CZTS- SO_4 Film	128
5.4.7	Optical Properties of The CZTS Films Prepared Using Different Salt Precursors	129
5.4.8	Composition Of The CZTS Thin Films Prepared Using Different Salt Precursors	131
5.4.9	Electrical Properties of The CZTS Thin Films Prepared Using Different Salt Precursors	132
5.4.10	Solar cell Devices Based on CZTS Thin Films Prepared Using Different Salt Precursors	134

5.5	Influence of Precursor Thin Films Stacking Order on The Properties of $\text{Cu}_2\text{ZnSnS}_4$ Thin Films Fabricated by Electrochemical Deposition Method	136
5.5.1	Cyclic Voltammograms and Surface Morphology Images	136
5.5.2	XRD Peaks For A CZTS Thin Film With Different Precursor Stacking Order	137
5.5.3	Raman Spectra Of CZTS Thin Films With Different Precursor Stacking Orders	139
5.5.4	Morphology Images And Cross-Sections of CZTS Thin Films in Different Stacking Orders	141
5.5.5	Compositional Analysis Of CZTS Thin Films With Different Precursor Stacking Order	142
5.5.6	Cross-Section Of Stacking Order A (Cu/Sn/Cu/Zn)	143
5.5.7	Optical properties of CZTS thin films with different precursor stacking orders	144
5.5.8	Electrical Properties of CZTS Thin Films	146
5.5.9	Photovoltaic Device Of The CZTS Solar Cells Using Different Precursor Stacking Order	147
5.6	Summary	148
	CHAPTER 6: RESULTS AND DISCUSSION : CZTS Solar Cell	151
6.1	Introduction	151
6.2	Influence of Substrate Temperature on The Properties of Electrochemical deposition of Kesterite $\text{Cu}_2\text{ZnSnS}_4$ (CZTS) Thin Films For Photovoltaic Applications	151
6.2.1	XRD Patterns of CZTS thin Films Prepared at Different Substrate Temperatures	152
6.2.2	Raman Spectroscopy of CZTS Thin Films Sulfurized at Various Substrate Temperatures	153
6.2.3	Surface Morphologies of CZTS Films Sulfurized at Various Substrate Temperatures	154

6.2.4	Chemical Composition of The CZTS Films Sulfurized at Various Temperatures	156
6.2.5	Electrical Properties of The CZTS Films	158
6.2.6	Elemental-Composition Maps of CZTS Solar Cell	159
6.2.7	Cross-Sectional Images of The Solar Cell	160
6.2.8	Optical Properties of The CZTS Films Sulfurized at Different Substrate Temperatures	161
6.2.9	CZTS Solar Cell Device Efficiency	163
6.3	Dependence of The Properties of Copper Zinc Tin Sulfide Thin Films Prepared by Electrochemical Deposition on Sulfurization Temperature	165
6.3.1	Cyclic Voltammogram of The Electrochemical Deposition of CZT Films	165
6.3.2	XRD Patterns of The Annealed CZTS Thin Films Prepared in Different Sulfurization Temperatures	166
6.3.3	Raman Spectra of The CZTS Thin Films Prepared in Different Sulfurization Temperatures	168
6.3.4	The Surface Morphology of CZTS Thin Films Annealed Different Sulfurization Temperatures	169
6.3.5	FE-SEM Image of The Cross Section of A CZTS Film Sulfurized at 400 °C	171
6.3.6	Chemical Compositions of The CZTS Thin Films	172
6.3.7	Optical Properties of The CZTS Films Prepared at Different Sulfurization Temperatures	174
6.4	Summary	176
 CHAPTER 7 :AQUEOUS SYNTHESIS CUBOID, CUBIC $\text{Cu}_2\text{ZnSnS}_4$ (CZTS) NANOCRYSTALS BY SOLVOTHERMAL SYNTHESIS		 179
7.1	Introduction	179

7.2	Solvent Solution-Dependent Properties of Nonstoichiometric Cubic $\text{Cu}_2\text{ZnSnS}_4$ Nanoparticles	179
7.2.1	XRD Patterns of CZTS Nanocrystals Prepared With Different Solvent Solutions	180
7.2.2	Raman Spectrum of CZTS Nanocrystals Prepared With Different Solvent Solutions	181
7.2.3	TEM Image of The CZTS Nanocrystals Prepared Using OLA As Solvent Solution	183
7.2.4	Elemental Map of CZTS Nanocrystals	184
7.2.5	Optical Properties of CZTS Nanocrystals	185
7.2.5	CZTS Nanocrystals Solar Cell Device	186
7.3	Aqueous Synthesis of Visible-Light Photoactive Cuboid $\text{Cu}_2\text{ZnSnS}_4$ Nanocrystals Using Rotary Evaporation	188
7.3.1	XRD Patterns Of The $\text{Cu}_2\text{ZnSnS}_4$ Nanocrystals Preparing Using Different Rotations Rates	188
7.3.2	Raman Spectra of The $\text{Cu}_2\text{ZnSnS}_4$ Nanocrystals Preparing Using Different Rotations Rates	189
7.3.3	TEM Images of CZTS Nanocrystals	190
7.3.4	Optical Properties of CZTS Nanocrystals	191
7.4	Summary	192
	CHAPTER 8 :CONCLUSIONS AND RECOMMENDATIONS FOR FUTURE WORK	195
8.1	Conclusions	195
8.2	Recommendations For Future Work	199
	REFRENECES	201
	APPENDIXES	216
	Appendix 1	216

LIST OF TABLES		Page
Table 3.1	Overlapping XRD peak positions of CZTS and secondary phases	28
Table 3.2	Raman shifts for CZTS and relevant phases	30
Table 5.1	Crystallite size in film as variation in triangle wave pulse at time (τ)	94
Table 5.2	Chemical compositions of CZTS thin films	99
Table 5.3	A comparison of the photovoltaic parameters of the CZTS solar cells	104
Table 5.4	Reduction potentials of annealed CZTS thin films prepared without and with complexing agents (CA)	109
Table 5.5	Composition of films deposited without and with complexing agents (CA) after sulfurization determined by EDS analysis.	113
Table 5.6	Electrical properties of CZTS films deposited using different complexing agents (CA).	117
Table 5.7	Photovoltaic parameters of CZTS solar cells	120
Table 5.8	Composition of films deposited using different salt precursors determined by EDS analysis	131
Table 5.9	Electrical properties of CZTS films deposited using different salt precursors	133
Table 5.10	Photovoltaic parameters of CZTS solar cells	134
Table 5.11	Chemical compositions of CZTS thin films for different precursor stacking order	143
Table 5.12	Electrical properties of annealed CZTS thin films with different precursor stacking orders	146
Table 5.13	A comparison of the photovoltaic parameters of the CZTS solar cells using different precursor stacking orders	147
Table 6.1	Chemical compositions of the deposited thin films sulfurized at different substrate temperatures	157

Table 6.2	Electrical properties of the CZTS thin films sulfurized at different substrate temperatures	158
Table 6.3	Photovoltaic parameters of solar cells made from CZTS sulfurized at different substrate temperatures	163
Table 6.4	chemical composition of CZTS thin films annealed different sulfurization temperatures	172

LIST OF FIGURES

		Page
Figure 1.1	Figure 1.1 Fraction of world energy consumption by type of energy source in 2011. The inset shows share of energy consumption among renewable energies in 2011	2
Figure 1.2	Shows the abundance and cost of copper, zinc, tin and sulfur compared with those of some elements that are currently used to make thin film solar cells. The lowest abundance and highest cost element among the latter is tin (4 ppm and \$3000/ton, respectively), which is still significantly better than the elements used in the current technologies (Cd, Te, In, Ga).	6
Figure 3.1	Schematic representations of the kesterite (a) and stannite (b) structures	24
Figure 3.2	Relationship between binary, ternary, and quaternary semiconductors to produce $\text{Cu}_2\text{ZnSnS}_4$, starting from a II–VI parent compound	25
Figure 3.3	Phase diagram of CZTS. This phase diagram assumes 50% sulfur	27
Figure 3.4	Schematic structure of typical CZTS solar cell	36
Figure 3.5	Energy band diagram of a CZTS-based heterojunction solar cell showing the band bending near the junction and schematic representation of photo-generation and separation of charge carriers	37
Figure 3.6	Schematic diagram of a typical electrodeposition setup consisting of a cathode and anode, electrolyte, and source of electricity	44
Figure 3.7	Schematic diagram of the reduction of Cu^{2+} on the cathode electrode	45
Figure 3.8	Schematic diagram of the electrodeposition of CZRS thin film containing appropriate electrolyte metal ions, an electrode (or substrate) where the deposition is desired (working electrode), a counter electrode (usually an inert metal such as Pt), a reference electrode (Ag/AgCl or a standard calomel electrode (SCE)), hot plate, computer, and a potentiostat or a galvanostat as a power source	47

Figure 3.9	Variation of applied potential during cyclic voltammetry	48
Figure 3.10	Typical cyclic voltammogram showing the important peak parameters	49
Figure 3.11	P–N junction diode in thermal equilibrium with zero bias voltage applied	51
Figure 3.12	Energy band diagram of p–n junction at equilibrium.	52
Figure 3.13	p–n junction illuminated by one photon. An electron-hole pair is generated and split by the built-in electric field	53
Figure 3.14	Determining the point of maximum power output from a current–voltage curve of a p–n junction under illumination (gray)	55
Figure 3.15	Effect of series resistance on the I-V characteristics of a solar cell	60
Figure 3.16	Effect of shunt resistance on the I-V characteristics of a solar cell	61
Figure 3.17	Equivalent circuit used to represent solar cells. It consists of a current source, a diode, a shunt resistor, and a series resistor	62
Figure 4.1	Electrodeposition cell with electrolyte solution, Ag/AgCl reference electrode, Pt mesh counter electrode, and Mo-coated glass substrate working electrode.	68
Figure 4.2	Photographs of (a) rotary evaporator and (b) three-necked flask used in the aqueous synthesis of $\text{Cu}_2\text{ZnSnS}_4$ nanocrystals	69
Figure 4.3	Photograph and schematic diagram of the centrifuge system	69
Figure 4.4	1. Horizontal tube furnace for sulfurization of CZS and (b) schematic diagram of the experimental setup for CZS sulfurization	71
Figure 4.5	d) The applied potential (V) (vs. Ag/AgCl) as a function of total deposition time (t) for different triangle wave pulse times (τ) of (a) 120 s, (b) 180 s, (c) 240 s, and (d) 300 s	76
Figure 4.6	Flow chart of CZTS thin film growth on soda lime glass substrate by electrochemical deposition	78
Figure 4.7	Photograph and schematic diagram of thermal evaporation system	79

Figure 4.8	Photograph and schematic of the basic RF sputtering process. A voltage is applied between the target and the substrate to accelerate argon ions into the target and eject target atoms. The target atoms deposit on the substrate, creating a thin film	80
Figure 4.9	Photograph and schematic diagram of X-ray diffraction (XRD) apparatus	82
Figure 4.10	Photograph and schematic diagram of the Raman spectroscopy apparatus	84
Figure 4.11	Photograph and schematic diagram of the field-emission scanning electron microscopy and energy dispersive spectroscopy apparatus	85
Figure 4.12	Photograph of the optical reflectometer	86
Figure 4.13	Photograph and schematic diagram of the Hall effect measurement apparatus. There are four contacts at the corners of the sample. The red lines show the Hall voltage across different points with variation of current and magnetic field polarities	88
Figure 4.14	Photograph and schematic diagram of the UV–Vis spectroscopy apparatus	89
Figure 4.15	Photograph and schematic diagram of the transmission electron microscopy (TEM) apparatus	90
Figure 4.16	Image of the solar simulator and schematic diagram of the solar cell I–V measurement system	91
Figure 5.1	Cyclic voltammogram of the aqueous solution containing 0.04 mol/L CuCl_2 , 0.02 mol/L ZnCl_2 , 0.02 mol/L SnCl_4 , 0.1 mol/L lactic acid, Tri-sodium citrate ($\text{C}_6 \text{H}_5 \text{Na}_3 \text{O}_7$, 0.14 mol/L), scanned from -1.5 to 1.5 V at a rate of 10 mVs^{-1} (vs. Ag/AgCl) before starting deposition	92
Figure 5.2	XRD patterns of CZTS films deposited using different triangle wave pulse times 120, 180, 240 or 300 s and then annealed at 580°C for 2 h	93
Figure 5.3	Raman spectra of the CZTS thin films deposited using different triangle wave pulse times and subsequently annealed at 580°C for 2 h	95
Figure 5.4	FESEM images of the CZTS films sulfurized at 580°C for 2 h. Films deposited using different triangle wave pulse times:	97

(a) 120 s, (b) 180 s, (c) 240 s, (d) 300 s

Figure 5.5	Cross-sectional FESEM images of Glass/Mo/CZTS/CdS/ZnO/ITO solar cell device	98
Figure 5.6	EDX spectra of the CZTS thin film prepared using a pulse time of 300 seconds	100
Figure 5.7	Schematic showing how CZTS growth depends on triangle wave pulse time	100
Figure 5.8	STEM - EDS elemental map of CZTS cross-section	101
Figure 5.9	Plot of the absorption coefficient of a CZTS thin film grown on an SLG substrate. Inset shows a plot of $(\alpha h\nu)^2$ vs. $h\nu$ used to estimate the band gap energy	103
Figure 5.10	Dark J–V characteristics of the CZTS/ZnO heterojunctions fabricated using different triangle wave pulse times	105
Figure 5.11	Illuminated J–V characteristics of Glass/Mo/CZTS/CdS/ZnO/ITO solar cells synthesized using different triangle wave pulse times. Structure of the solar cell is in the inset	106
Figure 5.13	(a-d).CVs (vs. Ag/AgCl) recorded at a scan rate of 10 mVs^{-1} of solutions at pH 4.75 containing $0.02 \text{ M CuSO}_4 \cdot 5\text{H}_2\text{O}$, $0.01 \text{ M ZnSO}_4 \cdot 7\text{H}_2\text{O}$, 0.02 M SnSO_4 , and (a) no complexing agent, (b) EDTA, (c) tartaric acid and (d) trisodium citrate	108
Figure 5.14	XRD patterns of films deposited using different complexing agents	110
Figure 5.15	Raman spectra of films deposited from baths with different complexing agents	112
Figure 5.16	EDX spectra of the CZTS thin film prepared using trisodium citrate as complexing agents	113
Figure 5.17	(a-d) FESEM surface images of CZTS thin films electrodeposited in (a) the absence of complexing agent, and with (b) EDTA, (c) tartaric acid, and (d) trisodium citrate	115

Figure 5.18	Optical absorption coefficients of CZTS thin films grown at 580°C. Inset are plots of $(\alpha h\nu)^2$ versus $h\nu$ of CZTS films grown using different complexing agents (CA)	116
Figure 5.19	Cross-sectional FESEM images of a CZTS thin film electrodeposited in the presence of trisodium citrate	118
Figure 5.20	J–V curves of CZTS solar cells under illumination recorded under AM15 (100 mW cm ²)	119
Figure 5.21	CVs of electrolytes containing different salts. (a) CZTS-NO ₃ , (b) CZTS-C ₂ H ₃ O ₂ , (c) CZTS-Cl and (d) CZTS-SO ₄ . Scans were performed in the range of 0 to –1.2 V at a scan rate of 10 mV s ⁻¹	122
Figure 5.22	XRD patterns of CZTS films deposited using different salts and sulfurized at 580°C for 2h in sulfur atmosphere	124
Figure 5.23	Raman spectroscopy of the CZTS thin films prepared using different salt precursors	126
Figure 5.24	FESEM images of (a) CZTS- NO ₃ , (b) CZTS-C ₂ H ₃ O ₂ , (c) CZTS-Cl and (d) CZTS-SO ₄ films	127
Figure 5.25	STEM-EDXS mapping of the elements of CZTS-SO ₄ thin film sulfurized at 580 °C for 2h in sulfur atmosphere	128
Figure 5.26	The cross-sectional FESEM image of the CZTS solar cell prepared for the CZTS-SO ₄ thin film	129
Figure 5.27	UV-vis spectra of CZTS thin films deposited from electrolytes containing different salts. The inset shows plots of $(\alpha h\nu)^2$ versus $h\nu$ (eV) for the CZTS thin films	130
Figure 5.28	EDX spectra of the sample CZTS-SO ₄	132
Figure 5.29	Illuminated J-V characteristics (AM1.5G filter, 100 mW cm ⁻²) of the CZTS solar cells prepared from CZTS thin films fabricated from different precursor salts	135
Figure 5.30	FESEM surface micrographs and cyclic voltammograms (vs. Ag/AgCl) of (a, d) Cu, (b, e) Zn, and (c, f) Sn	137
Figure 5.31	X-ray diffraction patterns of the stacked precursor thin films	138
Figure 5.32	Raman scattering analysis of the stacked precursor thin films	140

Figure 5.33	Surface and cross-sectional FESEM images of CZTS thin films stacked as follows: Cu/Sn/Cu/Zn (stacking A), Cu/Zn/Cu/Sn (stacking B), Zn/ Cu/Sn/Cu (stacking C), and Sn/Cu/Zn/Cu (stacking D)	142
Figure 5.34	EDX spectra of the Cu/Sn/Cu/Zn (stacking A)	143
Figure 5.35	FESEM images of a broken cross-section for Cu/Sn/Cu/Zn (stacking A)	144
Figure 5.36	Optical absorption coefficients and plots of $(\alpha h\nu)^2$ vs. photon energy ($h\nu$) of the annealed CZTS thin films using different precursor stacking orders	145
Figure 5.37	Illuminated and dark J–V curves of solar cells fabricated from CZTS films grown with stacking order A: Cu/Sn/Cu/Zn measured under the irradiance of AM 1.5G full sunlight (100 mW cm^{-2}) with a cell active area of 1.0 cm^2	148
Figure 6.1	XRD patterns of electrodeposited CZTS thin films, sulfurized at various substrate temperatures	152
Figure 6.2	Raman scattering spectra of precursor films sulfurized at various substrate temperatures	154
Figure 6.3	FESEM images of CZTS films sulfurized at substrate temperatures of (a) 460, (b) 500, (c) 540, and (d) 580 °C	155
Figure 6.4	EDX spectra of the CZTS thin film sulfurized at substrate temperature 580°C	157
Figure 6.5	Crystallite size and resistivity of CZTS thin films sulfurized at different substrate temperatures	159
Figure 6.6	EDS elemental composition map of the CZTS cross-section sulfurized at a substrate temperature of 580 °C	160
Figure 6.7	Cross-sectional FESEM micrographs of a solar cell made from CZTS sulfurized at a substrate temperature of 580 °C	161
Figure 6.8	UV–Vis absorption spectra of CZTS thin films sulfurized at various substrate temperatures. Insert: Plot of $(\alpha h\nu)^2$ vs. $h\nu$, used to estimate the band gap energy	162
Figure 6.9	Light current density–voltage curves of the best-performing CZTS solar cells, recorded under AM 1.5 (100 mW/cm^2),	164

°C) illumination

Figure 6.10	Cyclic voltammogram of electrolyte containing copper chloride, zinc chloride and tin chloride measured for 60 min at room temperature	166
Figure 6.11	XRD patterns of the CZTS samples sulfurized at 250, 300, 350 and 400 °C	167
Figure 6.12	Raman spectra of CZTS thin films annealed using different sulfurization temperatures	169
Figure 6.13	FE-SEM images of CZTS films sulfurized at (a) 250 °C, (b) 300 °C, (c) 350 °C, and (d) 400 °C	170
Figure 6.14	FE-SEM image of the cross-section of the CZTS layer fabricated at a sulfurization temperature of 400 °C.	172
Figure 6.15	EDX spectra of the CZTS thin film prepared under sulfurization temperature 400 °C	173
Figure 6.16	Elemental ratios of CZTS thin films prepared at different sulfurization temperatures	174
Figure 6.17	Absorption spectra of CZTS thin films prepared at different temperatures. The inset shows $(\alpha h\nu)^2$ versus photon energy ($h\nu$) of the same CZTS thin films	176
Figure 7.1	XRD patterns of the prepared $\text{Cu}_2\text{ZnSnS}_4$ powders using different solvent solutions, including polyvinylpyrrolidone (CZTS-PVP), ethylene glycol (CZTS-EGL), oleylamine (CZTS-OLA) and ctadecene(CZTS-ODE	180
Figure 7.2	Raman spectra of CZTS powders prepared using different solvent solutions, including polyvinylpyrrolidone (CZTS-PVP), ethylene glycol (CZTS-EGL), oleylamine (CZTS-OLA) and octadecene (CZTS-ODE)	182
Figure 7.3	TEM images of $\text{Cu}_2\text{ZnSnS}_4$ nanocrystals. (a) The CZTS nanocrystals have an average size of about 60 nm. (b) The SAED pattern can be indexed to CZTS. (c) The HR-TEM image shows interplanar spacings of 3.0 Å, corresponding to the (112) plane.	184
Figure 7.4	(Top) FE-SEM image of the cross-section and (Lower) STEM EDX elemental maps of the cross-section of CZTS	185

nanocrystals in a solar cell device based on CZTS-OLA as a p-type absorber layer. The yellow line in the top image indicates the area containing the CZTS nanocrystals

Figure 7.5	The UV–Vis absorption spectrum of the CZTS-OLA. (Inset) Plot of the dependence of $(\alpha h\nu - hv)^2$ upon $h\nu$ for the CZTS nanocrystals (solid line), revealing a band gap of 1.48 eV (dotted line)	186
Figure 7.6	J–V characteristics under air mass 1.5 illumination, 100 mW/cm ² . (inset) FE-SEM image (from Fig. 4) of a typical solar cell based upon the CZTS-OLA nanocrystals	187
Figure 7.7	XRD patterns for as-synthesized CZTS nanocrystals produced using various rotations rates (40, 60, 80, and 100 rpm)	189
Figure 7.8	Raman spectra for as-synthesized CZTS nanocrystals produced using various rotations rates (40, 60, 80, and 100 rpm)	190
Figure 7.9	TEM image (a), SAED pattern (b), and HRTEM image (c) of the CZTS nanocrystals obtained at 100 rpm	191
Figure 7.10	UV–vis absorption spectrum for the CZTS nanocrystals. The inset shows a typical Tauc plot giving an estimation of the direct band gap energy of the CZTS nanocrystals obtained at 100 rpm	192

LIST OF SYMBOLS

T	Absolute temperature
α	Absorption coefficient
A	Area
D	Average crystal size
K	Boltzmann constant
μ	Carrier mobility
E_C	Conduction band edge
σ	Conductivity
R_c	Contact resistance
η	conversion effective
m^*	Effective mass
E_F	Fermi level of semiconductor
F	Force
n	Free electron concentration
p	Free hole concentration
ν	Frequency
R_H	Hall coefficient
V_H	Hall voltage
m_p	Hole effective mass
μ_p	Hole mobility
n	Ideality factor
P_{in}	Incident solar power
θ	Incident/Diffraction angle
d	Interplanar spacing of the crystal planes

a	Lattice constant along x-axis
c	Lattice constant along z-axis
I_m	Maximum current
J_m	Maximum current density
P_m	Maximum output power
Φ_m	Metal work function
$(hkil)$	Miller indices
h	Planck's constant
R	Resistance
ρ	Resistivity
A^{**}	Richardson's constant
I_o	Saturation current
ϕ_B	Schottky barrier height
E_g	Semiconductor band gap
R_s	Series resistance
I_{SC}	Short circuit current
J_{SC}	Short circuit current density
R_{sh}	Shunt resistance
t	Thickness
τ	Time
E_v	Valence band edge
V	Voltage
λ	Wavelength
w	Width

LIST OF MAJOR ABBREVIATIONS

AM1.5G	Air Mass 1.5 Global
Ar	Argon
CB	Conduction Band
CBD	Chemical Bath Deposition
CdS	Cadmium Sulfide
CE	Counter Electrode
CIGS	Copper Indium Gallium Sulfide ($\text{Cu}_2 \text{ZnSnS}_4$)
CTS	Copper Tin Sulfide (Cu_3SnS_4)
Cu	Copper
$\text{Cu}_2 \text{S}$	Copper (I) Sulfide
CuS	Copper (II) Sulfide
CZTS	Copper Zinc Tin Sulfide ($\text{Cu}_2\text{ZnSnS}_4$)
CZTS-PVP	CZTS synthesized with the solvent polyvinylpyrrolidone
CZTS-EGL	CZTS synthesized with the solvent ethylene glycol
CZTS-OLA	CZTS synthesized with the solvent oleylamine
CZTS-ODE	CZTS synthesized with the solvent octadecene
CZTSe	Copper Zinc Tin Selenide ($\text{Cu}_2 \text{ZnSnSe}_4$)
CZTSSe	Copper Zinc Tin Sulfide Selenide ($\text{Cu}_2 \text{ZnSn}(\text{S}_x \text{Se}_{1-x})_4$)
EDA	Electrodeposition and annealing
EDX	Energy Dispersive X-Ray Spectroscopy
Eq	Equation
FF	Fill factor

FWHM	Full Width at Half Maximum
HCl	Hydrochloric acid
HRTEM	High-resolution transmission electron microscopy
H ₂ S	Hydrogen Sulfide
TO	Tin doped indium oxide
IV	Current-voltage characteristics
JCPDS	Joint Committee on Powder Diffraction Standards
J-V	Current density - Voltage
KCN	Potassium Cyanide
KOH	Potassium hydroxide
MS	Metal semiconductor
Mo	Molybdenum
MoS ₂	Molybdenum disulfide
Mo -SLG	Soda-Lime glass coated with molybdenum
N ₂	Nitrogen gas
NCs	Nanocrystals
nm	Nanometer
O	Oxygen
PV	Photovoltaic
RE	Reference electrode
RF	Radio frequency
RPM	Rotation per minute
RT	Room temperature
S	Sulfur

SAED	Selected Area Electron Diffraction
SCR	Space Charge Region
Se	Selenium
SEM	Scanning Electron Microscopy
Sn	Tin
SnS	Tin sulfide
STEM	Scanning Transmission Electron Microscopy
TCO	Transparent Conductive Oxide
TEM	Transmission Electron Microscopy
TFSC	Thin Film Solar Cell
UV–Vis	Ultraviolet–visible
VB	Valence Band
WE	Working electrode
XRD	X-ray diffraction
Zn	Zinc
ZnO	Zinc oxide
ZnO: Al	Aluminum doped zinc oxide
ZnS	Zinc sulfide

LIST OF PUBLICATIONS

International Journals (total IF =26.76)

1. **E. M. Mkawi**, K Ibrahim, M K M Ali, M A Farrukh, A S Mohamed, Influence of triangle wave pulse on the properties of $\text{Cu}_2\text{ZnSnS}_4$ thin films prepared by single step electrodeposition, *Solar Energy Materials and Solar Cells* 130 (2014) 91–98. IF 5.03.
2. **E. M. Mkawi**, K. Ibrahim, M.K.M. Ali, M.A. Farrukh, Nageh K.Allam, Influence of precursor salts on the properties of electrodeposition of Cu-Zn-Sn metal precursors and corresponding $\text{Cu}_2\text{ZnSnS}_4$ -based solar cells ,*Solar Energy Materials and Solar Cells* ,Accepted manuscript. **IF 5.03**.
3. **E. M. Mkawi**, K. Ibrahim, M.K.M. Ali, M.A. Farrukh, Nageh K.Allam, Effect of complexing agents on the electrodeposition of Cu-Zn-Sn metal precursors and corresponding $\text{Cu}_2\text{ZnSnS}_4$ -based solar cells, *Journal of Electroanalytical Chemistry* 735 (2014) 129–135. **IF 2.87**.
4. **E. M. Mkawi**, K. Ibrahim, M.K.M. Ali, K.A.M. Saron, M.A. Farrukh, A.S. Mohamed, Nageh K.Allam, Aqueous synthesis of visible-light photoactive cuboid $\text{Cu}_2\text{ZnSnS}_4$ nanocrystals using rotary evaporation, *Materials Letters* 125 (2014)195–197. **IF 2.27**.
5. **E. M. Mkawi**, K.Ibrahim, M.K.M Ali, M.A.Farrukh, A.S.Mohamed, Dependence of the properties of copper zinc tin sulfide thin films prepared by electrochemical deposition on sulfurization temperature, *Journal of Materials Science Materials in Electronics* 25 (2014) 857-863. **IF 1.97**.
6. **E. M. Mkawi**, K. Ibrahim, M.K.M. Ali, M.A. Farrukh, Nageh K.Allam, Solvent Solution-Dependent Properties of Nonstoichiometric Cubic $\text{Cu}_2\text{ZnSnS}_4$ Nanoparticles, *Chemical Physics Letters* 608 (2014) 393–397. IF 1.99.
7. **E. M. Mkawi**, K. Ibrahim, M.K.M. Ali, M.A. Farrukh, Nageh K.Allam, Influence of precursor thin films stacking order on the properties of $\text{Cu}_2\text{ZnSnS}_4$ thin films fabricated by electrochemical deposition method, *Superlattices and Microstructures* 76 (2014) 339–348. **IF 1.98**.
8. **E. M. Mkawi**, K. Ibrahim, M.K.M. Ali, K.A.M. Saron, M.A. Farrukh, Nageh K.Allam, Influence of substrate temperature on the properties of

electrodeposited kesterite $\text{Cu}_2\text{ZnSnS}_4$ (CZTS) thin films for photovoltaic applications, *Journal of Materials Science: Materials in Electronics* 26(2015) 222–228. **IF 1.97**.

9. **E. M. Mkawi**, K. Ibrahim, M.K.M. Ali, A S Mohamed, Dependence of Copper Concentration on the Properties of $\text{Cu}_2\text{ZnSnS}_4$ Thin Films Prepared by Electrochemical Method , *International journal of electrochemical science* 8 (2013) 359-368. **IF 1.98**.
10. **E. M. Mkawi**, K Ibrahim, M K M Ali, M A Farrukh, A S Mohamed, Electrodeposited ZnS precursor layer with improved electro-optical properties for efficient $\text{Cu}_2\text{ZnSnS}_4$ thin film solar cells, *Journal of Electronic Materials*, Accepted manuscript. **IF 1.67**.
11. E. M. Mkawi, K Ibrahim, M K M Ali, M A Farrukh, A S Mohamed, Synthesized and Characterization of $\text{Cu}_2\text{ZnSnS}_4$ (CZTS) Thin Films Deposited by Electrodeposition Method, *Applied Mechanics and Materials* 343 (2013) 85-89. **IF -**.
12. **E. M. Mkawi**, K Ibrahim, M K M Ali, M A Farrukh, A S Mohamed, The effect of dopant concentration on properties of transparent conducting Al-doped ZnO thin films for efficient $\text{Cu}_2\text{ZnSnS}_4$ thin film solar cells prepared by electrodeposition method ,*Applied Nanoscience*, Accepted manuscript. **IF -**.

Conferences

1. **E.M. Mkawi**, K. Ibrahim ,M. K. M. Ali. M. A. Farrukh and Abdussalam Salhin Mohamed - Synthesized and characterization of $\text{Cu}_2\text{ZnSnS}_4$ (CZTS) thin films deposited by electrodeposition method, the 2013 2nd International Conference on Sustainable Construction Materials and Computer Engineering (ICSCMCE 2013) June 1-2, 2013, Singapore.

Cu₂ZnSnS₄ (CZTS) FILEM TIPIS DITUMBUHKAN DENGAN ELEKTROKIMIA ENDAPAN UNTUK SURIA SEL

ABSTRAK

Sejak beberapa tahun kebelakangan ini, sebatian kuantenari Cu₂ZnSnS₄ (CZTS) menjadi tarikan sebagai bahan baru yang tidak toksik dan berkos rendah, dengan sifatnya yang amat sesuai bagi aplikasi filem atau saput nipis fotovoltan (PV). Dalam tesis ini, satu kaedah pemprosesan larutan berkos- efektif dibangunkan bagi penyerap saput nipis CZTS melalui pemendapan elektrokimia prekursor Cu, Zn, dan Sn pada substrat molibdenum (Mo)-bersalut kaca kapur soda (soda-lime glass,SLG), diikuti dengan rawatan haba dalam atmosfera sulfur. Kesan daripada parameter elektrokimia yang pelbagai terhadap sifat dan pertumbuhan saput nipis CZTS juga dikaji . Keputusan menunjukkan bahawa sifat saput nipis. Pengaruh denyut gelombang segi tiga terhadap sifat saput nipis mampu meningkatkan struktur dan morfologi sifat sampel melalui peningkatan peluang bagi elemen yang berlainan bersentuhan. Di samping itu, penggunaan trisodium sitrat sebagai agen pengkompleksan dalam larutan elektrolit dapat mengurangkan perbezaan di antara puncak penurunan Zn dan Cu sehingga 0.25 V. Kewujudan garam sulfat dalam elektrolit memudahkan pengurangan ion logam, dan meningkatkan penghasilan saput nipis. Empat prekursor berbeza yang terdapat dalam keadaan berjujukan dikaji dan tertib prekursor ditemui mempunyai kesan yang signifikan terhadap sifat saput nipis yang terhasil. Pengaruh suhu penyepuhlindapan (420–580 °C), suhu pensulfuran (250–400 °C), dan atmosfera (N₂ dan Ar (5%)) terhadap morforlogi dan struktur sifat saput CZTS yang terhasil dikaji. Penyepuhlindapan dalam atmosfera N₂ didapati

perlu bagi pertumbuhan bijirin. Penggunaan kimia prekursor yang sama, sintesis akueus daripada nanohablur $\text{Cu}_2\text{ZnSnS}_4$ kubik dan kuboid melalui sintesis solvohaba penyejatan putaran dikaji untuk mengesahkan keadaan penghabluran, jurang-jalur dan penyerapan secara langsung, dan ruang antar-satah daripada CZTS jenis -P. Pencirian sampel yang optimum (disimpan dengan sitrat trisodium) melalui belauan sinar X (XRD) menunjukkan orientasi pada satah (112), (220), (200) dan (312), mengesahkan struktur kesterit CZTS. Sampel mempunyai morfologi padat yang homogen, tanpa sebarang retak, dan saiz bijirin melebihi $1.5 \mu\text{m}$. Pekali penyerapan saput adalah melebihi 10^4 cm^{-1} dan jurang-jalurnya meningkat kepada 1.48 eV . Kepekatan dan kelincahan saput CZTS adalah $4.5 \times 10^{20} \text{ cm}^{-3}$ dan $3.79 \text{ cm}^2\text{V}^{-1}\text{S}^{-1}$. Sel suria terbaik dengan struktur peranti gelas /Mo/CZTS/CdS/ZnO/Al:ZnO/Al yang diterbitkan daripada saput CZTS mempamerkan kecekapan penukaran awal 2.94% . Kajian ini menunjukkan fabrikasi saput nipis pada substrat molibdenum (Mo)-bersalut kaca soda kapur (SLG) adalah bermungkinan melalui pemendapan elektrokimia dengan aplikasi yang berpotensi dalam fotovolta sel suria .

Cu₂ZnSnS₄ (CZTS) THIN FILM GROWN BY ELECTROCHEMICAL DEPOSITION FOR SOLAR CELL

ABSTRACT

Cu₂ZnSnS₄ (CZTS) quaternary compounds have attracted much attention in the last few years as an abundant new low-cost and non-toxic material with desirable properties for thin film photovoltaic (PV) applications. In this thesis, a cost-effective solution processing method is developed for the fabrication of CZTS thin film absorbers by electrochemical deposition of Cu, Zn, and Sn precursors on molybdenum (Mo)-coated soda-lime glass (SLG) substrate, followed by a heat treatment in sulfur atmosphere. The effects of varying the electrochemical deposition parameters on the properties and growth of the CZTS thin films were investigated. The influence of the triangle wave pulse on the properties of the CZTS thin films improves the structural and morphological properties of samples by increasing the opportunities for different elements to come into contact. Additionally, using trisodium citrate as the complexing agent in the electrolyte solution reduced the difference between the reduction peaks of Zn and Cu by up to 0.25 V. The presence of sulfate salts in the electrolyte led to easy reduction of the metal ions, and improved the thin film produced. Four different precursor stacking sequences were examined, and the ordering of the precursors was found to have a significant effect on the properties of the resulting thin films. The influence of the annealing temperature (420–580 °C), sulfurization temperature (250–400 °C), and atmosphere (N₂ and Ar (5%)) on the morphological and structural properties of the resulting CZTS films was

studied. Annealing in N₂ atmosphere was found to be necessary for grain growth. Using the same precursor chemistry, the aqueous synthesis of cubic and cuboid Cu₂ZnSnS₄ nanocrystals by rotary evaporation solvothermal synthesis was investigated to confirm the crystalline state, direct band gap and absorption, and interplanar spacing of p-type CZTS. Characterization of the optimized sample (deposited with trisodium citrate) by X-ray diffraction (XRD) revealed a preferred orientation of the (112), (220), (200) and (312) planes, confirming the kesterite structure of CZTS. The sample had a homogeneous, compact morphology without any voids or cracks, and the grain size was more than 1.5 μm. The absorption coefficient of the films was over 10⁴ cm⁻¹, and their band gap was increased to 1.48 eV. The carrier concentration and their mobility in the CZTS films were 4.5 × 10²⁰ cm⁻³ and 3.79 cm² V⁻¹ S⁻¹, respectively. The best solar cell with a device structure of glass/Mo/CZTS/CdS/ZnO/Al:ZnO/Al derived from the obtained CZTS film exhibited a preliminary conversion efficiency of 2.94%. The present study demonstrates the possibility of fabricating CZTS thin films on molybdenum (Mo)-coated soda-lime glass (SLG) substrates by electrochemical deposition with potential applications in photovoltaic solar cells.

CHAPTER 1

INTRODUCTION

1.1 The Energy Problem

According to recent studies, the global demand for energy is expected to increase by approximately 50% within the next 25 years. Fossil fuels such as natural gas, coal, and oil represent greater than 80% of world energy consumption. These fuels produce greenhouse gases upon combustion. In addition, the energy produced from these sources is becoming expensive. The search for sustainable alternatives is also driven by the increasing recognition that mankind's demand for energy is already causing changes in the climate that will have serious long-term consequences for the planet. For example, the energy sector produces 86.7% of the most greenhouse gases in the United States [1]. The most prevalent greenhouse gases are methane and carbon dioxide. These gases trap heat in the Earth's atmosphere by absorbing infrared radiation, which contributes to global warming [2]. Additionally, pollutant emissions, such as nitrous oxides and sulfur oxides, common to many fossil fuel sources have deleterious environmental effects and can lead to problems such as acid rain and smog. The fact that oil resources are expected to become exhausted within a relatively short period of time, the corresponding increase in prices of petroleum products, and the use of fossil fuel resources for political purposes will affect social and economic development worldwide [3]. Nuclear power plants also pose problems, related to fuel processing and the dumping of used fuel [4]. Electricity production is expected to continue to increase (from 17 PW h in 2009 to 28–35 PW h in 2035), and as a

consequence the increased demand on fossil fuels, as well as possible problems from CO₂ emissions, are bound to increase wholesale electricity costs [5].

What is needed to combat these issues is real renewable energy, i.e., technologies based on energy that is inexhaustible. Those available on earth are geothermal energy, energy from the interaction of the earth and moon (tidal forces), and solar energy. The latter can be subdivided in to hydropower, wind power, biomass/biofuel, and photovoltaic/solar thermal power plants/solar heating systems (all these forms of energy can eventually be traced back to creation by the sun, i.e., solar energy). Global fossil fuel consumption based on world production data as of 2011 is shown in Figure 1-1.

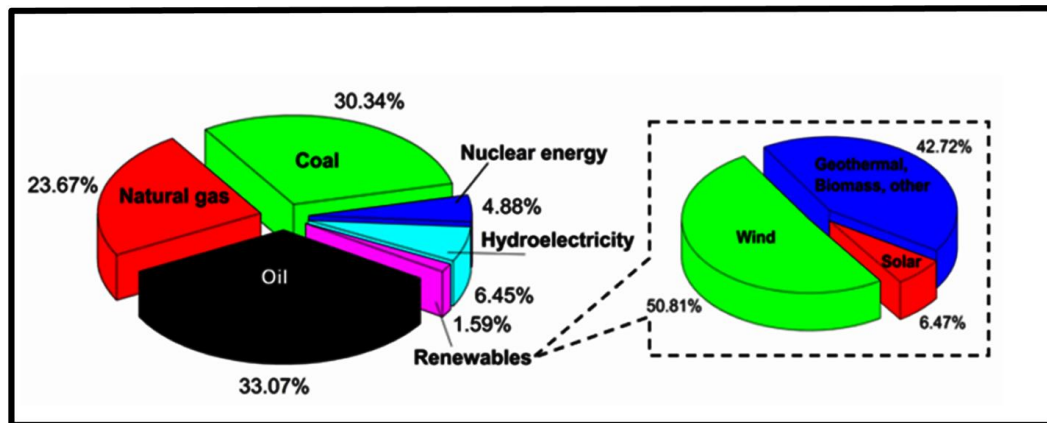


Figure 1.1 Fraction of world energy consumption by type of energy source in 2011. The inset shows share of energy consumption among renewable energies in 2011 [6].

1.2 Solar Energy

Solar energy is abundant, non-polluting, and able to provide a significant fraction of global energy demand. Current trends suggest that solar energy will play an essential role in future energy production. Perhaps the most promising renewable energy is solar energy, as it can potentially meet the world's energy consumption. Indeed, solar

energy alone has the capacity to meet all the planet's energy needs for the foreseeable future. The sun deposits ~120,000 TW of electromagnetic radiation on the surface of the Earth per year, a much greater amount than those of human needs. Covering just 0.16 % of the land on Earth with 10 % efficient solar conversion systems would provide 20 TW of power, which is nearly twice the world's present fossil fuel consumption (or the equivalent of 20,000 GW nuclear fission plants). However, photovoltaics have not yet reached so called grid parity, which means that electricity from solar cells is more expensive than energy from conventional sources like coal or gas. Consequently, further research is essential to increase the efficiency of solar cells and to make them cheaper. One approach for this is thin solar cells.

1.3 Thin Film Photovoltaics

Over recent years, the photovoltaics (PV) market has grown dramatically, and is completely dominated by products using silicon wafers. The two parameters often cited as the most important for solar cells are efficiency and cost. The cost of a Si solar cell is largely dependent on the cost of the Si wafer used in its fabrication. The high production cost and limited feedstock of silicon has sparked the photovoltaic community to search for new materials and technologies. Cheaper solar cells can only be produced using cheaper materials and low-cost fabrication methods. This is where thin film technology offers promising potential as an alternative to silicon photovoltaic technology [7]. Thin film solar cells are based on materials that strongly absorb sunlight, so that the cells can be very thin (1–3 μm), which reduces the demand for the raw material. The bottleneck for solar electricity to become a household energy source

is mainly its cost. The cost of the Si wafer accounts for over 50 % of the total module cost. To eliminate this high cost component, silicon wafers may be replaced by thin films of semiconductors deposited onto a supporting substrate [8]. The main motivation for thin film solar cells is ability for high productivity and high speed manufacturing and low cost by using minimum material requirements . In the case of thin film solar cells, much less material is used compared with that required for crystalline silicon solar cells. Because the absorption coefficient of typical thin film absorber materials is ~100 times higher than crystalline silicon, a 100 times thinner layer of thin film material can absorb an equivalent amount of energy as crystalline silicon. For example, while 100 cm^3 ($100 \mu\text{m} \times 1 \text{ m} \times 1 \text{ m}$) crystalline silicon may be needed for a 1 m^2 solar cell, only 1 cm^3 is needed for a 1 m^2 thin film cell. In addition, thin film solar cells are less susceptible to the purity and crystallinity of their materials, and so the requirements on thin film solar cell materials are less stringent than for crystalline silicon solar cells [9]. Thus, thin film solar cells are cheaper to produce than silicon solar cells. Another advantage of thin film solar cells is that they can be fabricated on flexible materials like metal foils or polyimides, which allows for completely new applications [10]. Yet another advantage is that it is possible to adjust the band gap of thin film materials by varying their composition. Thus, a larger portion of the solar spectrum can be used and higher efficiency can be achieved, because the theoretical possible efficiency depends strongly on the band gap. The huge reduction in the active material requirements with respect to those of the standard technology allows a large decrease in device costs. Moreover, the large versatility in the device design and fabrication, owing to the wide choice of different substrates

(rigid and flexible) and deposition techniques for the different device layers, allows precise engineering and optimization of the solar cell stack to enhance device performance [11]. Thin film PV has been therefore recognized as a promising strategy to obtain high efficiency and low cost PV devices, thus fulfilling the actual requirements of the increasing electrical demand.

1.4 Thin Film Photovoltaic Materials

Materials intended for thin film solar cells must fulfill some important conditions to be usable. The ideal materials should have high optical absorptivity to absorb sunlight (greater than 10^4 cm^{-1}). The term absorption coefficient can be defined as “the rate of decrease in the intensity of light as it passes through a given material”. An essential precondition is of course a large absorption coefficient, as all (suitable) light should be absorbed in only a few micrometers [12]. Furthermore, the band gap should be in the range of roughly 1.0–1.6 eV to provide the theoretical opportunity to reach sufficient efficiencies. The bandgap should also be appropriate, ideally around 1.5 eV, to absorb a significant portion of the solar spectrum. Also needed is the ability to form a good electronic p–n junction with compatible materials.

Nevertheless, not all potentially suitable compounds can be used to produce viable solar cell materials. Many other conditions, including availability, possibility of industrial scale production, cost, and environmental safety (e.g., toxicity), have to be fulfilled. Recently, chalcogenide thin-film photovoltaic (PV) materials such as CdTe, Cu(In,Ga)Se₂ (CIGS), Cu₂ZnSSe₄ (CZTSe), Cu₂ZnSnS₄ (CZTS), and Cu₂ZnSn(S,Se)₄ (CZTSS) have attracted great attention owing to their ability to produce high efficiency, low cost, large area thin film solar cells (chalcogens are defined as all

group 16 elements of the periodic table such as oxides, sulfides, tellurides and selenides).

Chalcogenide thin-film photovoltaics have seen significant improvements in device efficiency in the last 20 years, and have now reached mass production. In 2014, small area CIGS solar cells reached an efficiency of 20.9% (close to the record efficiency, 25 %, of bulk-crystalline Si solar cells [13]) and large-area modules with efficiency of about 13–14% are currently produced on an industrial scale. Even CdTe solar cells, which have a record efficiency of 10.1% for research cells and 16.1% for total area modules [14], already have an annual industrial production of more than 1.5 GW. Despite great developments in chalcogenide-based PVs, these technologies suffer from using toxic (Cd) and rare elements, such as In, Ga and Te, the high cost and scarcity of which could limit the sustainability of these technologies in the years to come [15]. Figure 1.3 shows the abundance of these materials in the earth’s crust and their cost.

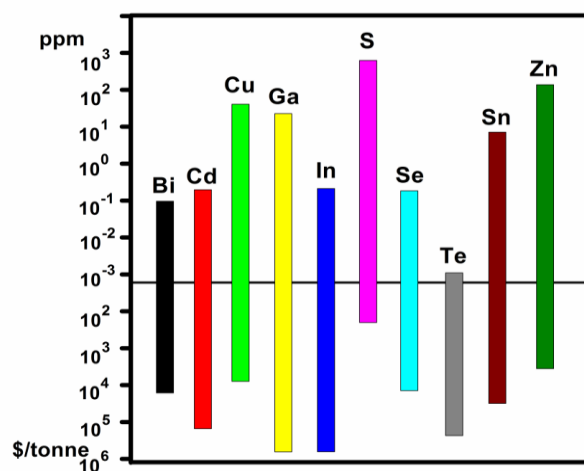


Figure 1.2 shows the abundance and cost of copper, zinc, tin and sulfur compared with those of some elements that are currently used to make thin film solar cells. The lowest abundance and highest cost element among the latter is tin (4 ppm and \$3000/ton, respectively), which is still significantly better than the elements used in the current technologies (Cd, Te, In, Ga) [16].

In the last decade, many efforts have focused on the development of a new class of quaternary compounds as possible candidates to replace CIGS in thin film solar cells. These materials can be thought of as a derivation of the CIGS chalcopyrite structure obtained by a process known as “cross-substitution”, consisting of the replacement of one element (In or Ga in the present case) with two elements of different groups in the periodic table chosen to keep the ratio between the number of atoms and valence electrons fixed. The resulting materials are therefore quaternary compounds given by the chemical formula $\text{Cu}_2\text{-II-IV-VI}_4$, where VI is a chalcogen element (S or Se) and II and IV represent divalent (Zn, Cd, Fe) and tetravalent (Sn, Ge, Si) elements, respectively. Among the possible $\text{Cu}_2\text{-II-IV-VI}_4$ compounds, kesterites $\text{Cu}_2\text{ZnSn(S,Se)}_4$ (CZTS(Se)) are the most studied, and the rapid improvement in their photovoltaic performance obtained in recent years makes them much more attractive. Considerable work has recently been carried out on kesterite $\text{Cu}_2\text{ZnSnS}_4$ (CZTS) to make it a good absorber layer for thin film solar cells and thermo-electric power generators [17, 18]. CZTS thin films are usually in a polycrystalline form consisting of kesterite crystal structures. CZTS has excellent physical properties, including a high optical absorption coefficient ($>10^{-4} \text{ cm}^{-1}$), direct band gap (1.4–1.5 eV), and low thermal conductivity. CZTS can be derived from the CIGS structure by the isoelectronic substitution of two In (or one In and one Ga) atoms by one Zn and one Sn atom. As a consequence, CZTS has some similar properties to those of CIGS. The availability of copper, zinc, tin and sulfur in the earth’s crust are much higher than that of indium (0.049 ppm [19], at 50, 75, 2.2. and 260 ppm, respectively, i.e., all the constituents of CZTS are abundant in the earth’s crust. Intrinsic point defects in CZTS make its conductivity p-type. The crystal structure of CZTS can tolerate some

deviation from stoichiometry, making its deposition process easier. Moreover, grain boundaries in CZTS thin films are beneficial in enhancing minority carrier collection [20]. Theoretical calculations have shown that a conversion efficiency as high as 32.2 % [21] is possible for CZTS thin film solar cells with a CZTS layer of a few micrometers. To date, most of the solar cell devices based on p-type CZTS have been fabricated by sputtering or evaporation followed by annealing and sulfurization at high temperature (300–550 °C). To reduce the cost of these cells, it is necessary to develop alternate processing methods for their fabrication, such as solution based or electrochemical techniques.

1.5 Research Objectives

The principal goal of this research is to develop CZTS-based thin-film solar cells grown onto Mo-coated glass substrates by electrochemical deposition method. The sub objectives of this project can be summarized in the following :

1. To determine the optimal growth parameters that influence the structural, optical, and electrical properties of $\text{Cu}_2\text{SnZnS}_4$ (CZTS) thin film structures grown on Mo-coated glass substrates by electrochemical deposition.
2. To investigate the effects of annealing conditions including substrate temperature and sulfurization temperature on the properties of $\text{Cu}_2\text{SnZnS}_4$ (CZTS) thin film.
3. To investigate the synthesis and fabrication of $\text{Cu}_2\text{SnZnS}_4$ (CZTS) nanoparticle structures and films by solvothermal and rotary evaporation techniques under different conditions.
4. To evaluate the performance of solar cells incorporating the obtained CZTS thin film and its dependence on the growth parameters.

1.6 Originality of The Research Work

The originality of the study is supported by the following points.

- a) The electrochemical deposition and growth of $\text{Cu}_2\text{ZnSnS}_4$ (CZTS) on Mo substrates is a new approach (the first report was published 5 years ago [22]). This technique could provide a new insight into the use of semiconductor materials with good properties for photovoltaic applications.
- b) This study is the first to report the use of triangle wave pulses to deposit CZTS thin film and its role in solving the problem of tin reduction during annealing treatment [23].
- c) This study is the first to report a decrease in reduction potential between Cu and Zn elements of 0.25 V when trisodium citrate is used as a complexing agent.
- d) This study is the first to report the effect of precursor salts on the stoichiometry of CZTS thin film.
- e) This study is the first to report the use of a three-zone furnace to fabricate CZTS thin films to prevent loss of S during annealing and optimization of sulfurization temperature.
- f) A review of contemporary studies of the synthesis of visible-light protective cubic $\text{Cu}_2\text{ZnSnS}_4$ nanocrystals and nonstoichiometric nanoparticles has not been conducted until now.

1.7 Outline of The Thesis

The thesis consists of eight chapters. An introduction to the energy problem, renewable energy, thin film materials, and $\text{Cu}_2\text{ZnSnS}_4$ (CZTS) thin film was presented in Chapter 1. This chapter also included the motivation, objectives and original contributions of this research, ending with this outline of the thesis. Chapter 2 consists of the literature review of the $\text{Cu}_2\text{ZnSnS}_4$ thin film deposition processes. In chapter 3, theoretical background of CZTS thin films, including its advantages, formation reactions, properties, and characteristics. PN Junctions and Solar Cells devices, principles of electrochemical deposition is discussed. Chapter 4 comprehensively describes the methodology and instrumentation used in the study. The results obtained from the research work are analyzed and discussed in Chapters 5, 6, and 7. Chapter 5 elaborates on the properties of Cu, Zn, and Sn metal precursors electrochemically deposited on Mo substrates under different conditions. Chapter 6 presents the results of investigations into the sulfurization and annealing treatment of the Cu, Zn, and Sn metal precursors under different conditions. Chapter 7 contains the experimental results of the synthesis of visible-light protective cubic $\text{Cu}_2\text{ZnSnS}_4$ nanocrystals and nonstoichiometric cubic $\text{Cu}_2\text{ZnSnS}_4$ nanoparticles via a rotary evaporation and solvothermal synthesis under different parameters. Chapter 8 is a summary of the work, in which important conclusions are highlighted. Future prospects of the work are also presented.

CHAPTER 2

LITERATURE REVIEW

2.1 Introduction

This chapter presents the history and a survey of the relevant literature concerning CZTS thin film solar cells and the evolution of the efficiency of CZTS thin film solar cells. This chapter also describes the background of a variety of techniques used for the deposition of CZTS thin films.

2.2 Evolution of CZTS Thin Film Solar Cell Efficiency

CZTS material was first introduced into solar cell applications in 1988 by Ito and Nakazawa. They successfully fabricated a heterodiode of CZTS and cadmium tin oxide (CTO) thin films on a stainless steel substrate [24]. That produced an open circuit voltage (V_{OC}) of 165 mV under AM1.5 illumination. Katagiri et al. [25] reported the fabrication of a CZTS thin film solar cell with the structure Mo/CZTS/CdS/ZnO:Al on soda lime glass substrate by sulfurization of electron beam deposited Cu/Sn/Zn stacked precursors. Their device showed a power conversion performance of 0.66% and an V_{OC} of 400 mV. In the same year, a best conversion efficiency of 2.3% and V_{OC} of 470 mV was achieved by Friedlmeier et al. [26] using CZTS as a good light absorber layer in a similar structure to that of Katagiri's device, prepared by the sulfurization of co-deposited Cu-Zn-Sn films. Katagiri et al. recorded a new CZTS device efficiency of 2.63% by varying the method of the sulfurization of the Cu/Sn/ZnS stacks [27]. The efficiency was increased to 5.45 % in 2003 by the same group using different annealing conditions [28]. And further improved to 6.7 %

in 2008 by soaking the thin films in deionized water to etch the metal oxide particles in the CZTS layer [29]. A CZTS thin film solar cell with a conversion performance of 9.6% was attained in 2010 by Mitzi et al., who used a hydrazine precursor solution and sulfurization to deposit CZTS active layers via a spin-coating technique [30]. and further improved the efficiency of their cell to 10.1 % in 2011[31]. Obtained by the same group, the most recent record efficiency of CZTS thin film solar cells is 11.1%, according to the available literature.

2.3 CZTS Thin Film Deposition Techniques

Different deposition methods have been used to fabricate CZTS thin films, including evaporation, sputtering, spin coating, and screen printing. These methods can be divided into two main categories, vacuum-based techniques and solution-based techniques. In this section these technique are reviewed.

2.3.1 Vacuum-Based Techniques

Vacuum based deposition techniques are popular methods of obtaining high quality thin film devices owing to the high uniformity of the produced films. These techniques include coating of the integral atoms of the CZTS material onto a substrate either by sputtering or by evaporation/co-evaporation of target sources under optimized conditions (pressure and temperature). The advantages of these techniques include the good and simple control of the chemical composition of the thin films, and good reproducibility. Nonetheless, the final CZTS thin films are normally obtained by high temperature sulfurization of the deposited stacks of metals, metal sulfides, or a

combination of the two. These procedures are usually slow and may require several hours for thin film growth and annealing.

2.3.1.1 Sputtering Techniques

Several sputtering techniques have been widely employed in previous studies to deposit CZTS thin films for solar cell applications such as argon beam, ion beam, DC, RF, hybrid, and reactive magnetron sputtering.

For example, Ito and Nakazawa used CZTS pressed targets to fabricate thin films by an argon beam sputtering technique without an annealing process. The resulting CZTS thin film had a stannite structure, a band gap of 1.45 eV, and an obtained V_{OC} of 165mV [25]. However, the efficiency of the device was not reported. Later on, Tanaka et al. [32] employed hybrid sputtering technology to deposit Sn/Zn/Cu precursor layers which were then annealed at different temperatures with sulfur flux. The CZTS phase formed at 350 °C. The produced films had a direct band gap of 1.5 eV, absorption coefficient higher than 10^4 cm^{-1} , and a high rate of Zn losing when heated over 450 °C. CZTS solar cells with an efficiency of 5.7% have been fabricated by reactive co-sputtering of Cu, SnS, and Zn in an atmosphere containing 20% concentrated H_2S by Katagiri et al [29]. The best performance of the resulting solar cell device was obtained at component material ratios of $\text{Cu}/(\text{Zn}+\text{Sn}) = 0.87$, $\text{Zn}/\text{Sn}=1.15$, and $\text{S}/(\text{Cu}+\text{Zn}+\text{Sn}) = 1.18$ [33]. Fernandes et al [34] used DC magnetron sputtering to deposit CZTS thin films and sulfurized them in N_2 atmosphere at 525 °C. Zhang et al.[35] formed CZTS thin films by sequential sputtering of Cu, Zn, and Sn from metallic targets using ion beam sputtering, then sulfurized the stacked Cu/Sn/Zn

precursors on soda lime glass (SLG) substrates without heating the substrates. Proper sulfurization was achieved in $S_2 + N_2$ flux at 550 °C for 3 h.

The best reported efficiency for sputtered CZTS solar cells is 7.6 %, obtained by Fukano et al [36]. This value was obtained by annealing at 580 °C for 30 min under 20 % H_2S balanced with N_2 . In addition, Fukano et al. also reported that CZTS films fabricated from a three-layer (ZnS/Sn/Cu (top)) precursor displayed higher quality than those obtained from a four-layer (ZnS/Sn/Cu/ ZnS (top)) precursor.

2.3.1.2 Evaporation

Evaporation techniques have been the preferred method of numerous academic researchers owing to previous achievements of good absorber materials using various evaporation technologies such as electron beam (EB) evaporation, co-evaporation, fast evaporation, and thermal evaporation. CZT precursors deposition by evaporation can be achieved by two different approaches:

- (i) single step simultaneous deposition of all precursors followed by sulfurization
- (ii) two step, sequential deposition of metallic precursors, e.g., Cu–Zn–Sn/Cu–Zn–Sn–Cu or Cu–ZnS–SnS, followed by sulfurization/annealing.

The first study of CZTS thin film fabrication by an evaporation technique was reported by Katagiri et al. in 1997 [25] They sulfurized Zn/Sn/Cu layers at 500 °C for 1–3 h under a $N_2 + H_2S$ (5%) atmosphere. The precursor layers were deposited by electron beam evaporation with a substrate temperature of 150 °C. A device with a structure of glass/Mo/CZTS/CdS/ZnO/Al produced from the resulting CZTS thin films exhibited a conversion efficiency of 0.66 %. Katagiri et al. also reported that replacing Zn with ZnS in the initial precursor stack significantly improved the

adhesion of the film material to the Mo/SLG substrate. This development offered solar cells with an efficiency of 5.45%, V_{OC} of 582 mV and short circuit current (J_{SC}) of 15.5 mA/cm [25]. Kobayashi et al.[33] used EB evaporation and sulfurized the resulting films at a temperature of 510–550 °C, and obtained a best efficiency of 4.53%, V_{OC} of 629 mV, J_{SC} of 12.53 mA/cm² and FF of 0.58 at 520 °C [37]. Wang et al. [38] used a thermal co-evaporation technique to deposit elements simultaneously onto the same substrate at 110 °C, and annealed them at 540 °C for 5 min in sulfur atmosphere. The produced solar cell with thickness of 650 nm and structure of glass/Mo/CZTS/CdS/i-ZnO/ITO/Ni–Al grids exhibited a V_{OC} of 587 mV, J_{SC} of 17.8 mA/cm², FF of 65 % and efficiency of 6.8 %. Tanaka et al [39], deposited CZTS thin films by co-evaporation of Cu, Zn, Sn, and S precursors and obtained growth along the [112] plane with an increasing grain size with substrate temperature between 400 and 600 °C. In a later study, they investigated the influence of CZTS thin film composition on the structure and electrical properties[40] . In another study, CZTS films deposited on Mo coated SLG substrates at 110 °C by thermal evaporation technique and annealed on a hot plate at 540 °C for 5 min were used to fabricate a solar cell device with a layer arrangement of SLG/Mo/CZTS/CdS/i-ZnO/Al:ZnO that displayed an efficiency of 6.8% , V_{OC} of 587 mV, J_{SC} of 17.8 mA/cm² and FF of 65% [38] . More recently, Shin et al.[41] deposited CZTS thin film based solar cells on Mo coated SLG substrates by a thermal evaporation method. After annealing at 570 °C for 5 min in air, the device showed an efficiency of 8.4%, V_{OC} of 661 mV, J_{SC} of 19.5 mA/cm² and FF of 65.8%.

2.3.1.3 Pulsed Laser Deposition Technique

Pulsed laser deposition (PLD) is one of the best methods of producing very good quality layers of complex compositions, and has advantages including simplicity, clean deposition (owing to the use of a high vacuum chamber), and deposition of highly enhanced crystal structures owing to the high energy and flexibility in the engineering plan.

Sekiguchi et al.[42] benefited from this technique to fabricate the first epitaxially grown CZTS films on GaP substrate. Moriya et al.[43] employed a KrF pulsed laser with a wavelength of 248 nm to form CZTS thin films for solar cell applications after annealing in N₂ atmosphere at different temperatures (300–500 °C), and obtained a efficiency of 1.74 % from a sample treated at 500 °C in 2007.

2.3.2 Solution-Based Techniques

The various vacuum techniques were the established methods of producing CZTS thin films for several decades, then the majority of researchers switched to low-cost deposition techniques (non-vacuum approaches) in subsequent years. Vacuum routes are mostly expensive and consume more time and energy than non-vacuum approaches, which are less costly, simpler, and offer high material output with lower time and energy cost. As a result, there has been a recent unexpected growth in CZTS thin films solar cell fabrication by non-vacuum techniques; therefore, solution-based fabrication will be an important direction for future research. These solution-based techniques are briefly described below.

2.3.2.1 Precursor-Ink Based Approach

The sol-gel method is the foremost of the ink-based approaches, and was first introduced as a method of fabricating CZTS thin films by Tanaka et al [44]. They prepared a CZTS solution by using the elemental powders of copper, zinc, tin and sulphur, with stirring at 45 °C for 1 h, and then spin-coated and dried the resulting film in air at 300 °C. This method was repeated by Yeh et al [45], who added an annealing process in N₂+H₂S atmosphere at 500 °C for 1 h and studied the effect of the preparation (synthesis and annealing) temperatures on the properties of the resulting CZTS thin films. In other work, Ki et al. spin-coated CZTS films from a solution of copper chloride, zinc chloride, tin chloride and thiourea dissolved in 70:30 deionized water/ethanol and stirred at 40 °C for 30 min. The spin-coated films were annealed at 580 °C for 2.5 min and used to fabricate a solar cell with a structure of glass/Mo/CZTS/CdS/ZnO/ITO/Ni-Al that exhibited an efficiency of 4.1% [46]. Todorov and his group reported the coating of crack-free CZTS films onto glass substrates by reacting metal salts (complexed with triethanolamine) with dissolved elemental sulfur in ethylene glycol at 170 °C for 3 h [47].

Zhou et al. [48] used a very easy and cheap technique known as screen printing (SP) to print CZTS layers from ink prepared from powders of copper, zinc, tin, and sulfur onto Mo coated polyimide. The resulting solar cell with the structure polyimide/Mo/CZTS/CdS/Al:ZnO/Al showed an efficiency of 0.49%, V_{OC} of 386 mV, J_{SC} of 4.76 mA/cm², and FF of 0.27.

Many previous works have reported the preparation of CZTS thin films by chemical bath deposition (CBD) methods, such as the fusing of Cu atoms into films by an ion exchange method [49], synthesis of nanocrystalline CZTS by a drop method [50],

synthesis of CZTS nanorods via controlled evaporation from a solution source [51], and synthesis of CZTS nanocrystals by high temperature arrested precipitation. In the last case, copper acetylacetonate, zinc acetate, tin chloride dehydrate, and elemental sulfur were reacted in oleyamine at 280 °C for 1 h under an inert atmosphere, and the solar cell fabricated from the obtained nanocrystals exhibited an efficiency of 0.23%, V_{OC} of 321 mV, J_{SC} of 1.95 mA/cm² and FF of 0.37 .

The most impressive result obtained for CZTS photovoltaics prepared by a solution based method was reported by Xin et al [52] .They fabricated a dye sensitized solar cell with N719 ruthenium based dye, a TiO₂ layer on FTO, a CZTS absorber layer on FTO, and an ionic liquid electrolyte that exhibited an efficiency of 7.37%, V_{OC} of 800 mV, J_{SC} of 17.7 mA/cm², and FF of 52.2%.

2.3.2.2 Spray Pyrolysis

The spray pyrolysis deposition (SPD) method is considered to have the greatest simplicity, easiest handling, and best reproducibility of the large area coating techniques. It can be a suitable method for industrial commercial production because it does not require a vacuum at any step of the fabrication process, which is the most pronounced advantage of the technique. In spite of these advantages, spray pyrolysis has not been widely used for the creation of CZTS thin films.

Nakayama and Ito [53] prepared CZTS thin films by a spray pyrolysis technique for the first time in 1996. They sprayed a solution of CuCl, ZnCl₂, SnCl₄, and thiourea dissolved in 50:50 DW/ethanol onto SLG substrates at temperatures from 280 to 360 °C. Prabhakar and Jampana [54] also used this method and determined the conductivity of the sprayed CZTS films, reporting that the conductivity increased with

Na-diffusion from SLG and Cu-deficiency in the sprayed CZTS. The effect of Na-diffusion was found to be stronger than that of Cu-deficiency, and the conductivity of the film increased by an order of magnitude when SLG was used instead of borosilicate glass.

2.3.2.3 Electrodeposition technique

Electrodeposition is one of most attractive solution-based techniques, and has been commonly applied to the growth of solar cell absorber layers of several materials, such as CdTe, CZTS and CIGS [54, 55]. The preparation of CZTS thin films by electrodeposition is usually achieved in one of two ways, namely the sequential electroplating of precursors or the single step electrodeposition of precursors. Both of these are followed by sulfurization using different sulfur sources, such as pure S vapor, S_2+N_2 and S_2+Ar , at annealing temperatures between 300 and 600 °C. The first CZTS film solar cell prepared by an electrochemical deposition method was reported by Scragg et al., with efficiency of 0.8%. Electrochemically deposited metal stack Zn/Sn/Cu was sulfurized by S vapor at 550 °C for 2 h. They added that the low efficiency of the obtained solar cell was caused by a high series resistance and a high shunt conductance [22].

Araki et al. [56] synthesized CZTS thin films by annealing co-electrodeposited Cu-Zn-Sn films in S atmosphere for 2 h. Slightly Zn-rich films gave the best device efficiency, 3.16%. Copper (II) sulfate pentahydrate, zinc sulfate heptahydrate, tin (II) chloride dihydrate, and tri-sodium citrate dihydrate were used for the co-electrodeposition. The co-electrodeposited films did not exhibit any phase separation after annealing.

Ennaoui et al.[57] reported a novel low cost technique for the preparation of CZTS thin film absorber layers for solar cell applications. First, they prepared Cu–Zn–Sn precursor layers on Mo coated SLG substrates using single step electrochemical deposition from an alkaline electrolyte bath containing Cu(II), Zn(II), and Sn(IV) metal salts, which were further reacted with Ar/H₂S to form CZTS thin films. A solar cell fabricated using these CZTS thin films with the configuration glass/Mo/CZTS/CdS/ZnO/Ni–Al showed an efficiency of 3.4% ($V_{OC} = 563$ mV, $J_{SC} = 14.8$ mA/cm² and FF = 41%).

Pawar et al. [58] demonstrated a single step co-electrodeposition of S along with the CZTS component metals from CuSO₄, ZnSO₄, SnSO₄, and Na₂S₂O₃ (sulfur source) in an aqueous electrolytic bath at room temperature. The as-deposited films were annealed in an Ar atmosphere at 550 °C for 1 h for grain growth, and did not require any post deposition sulfurization step. The bandgap of the film annealed at 550 °C was found to be 1.50 eV.

Ahmed et al.[59] developed a three-step method: i) sequential electroplating of Cu/Zn/Sn or Cu/Sn/Zn stacks; ii) annealing of the stacks at low temperature (210–350 °C) under N₂ to produce homogeneous alloys; iii) annealing of these well-mixed CuZn and CuSn alloys at 550–590 °C in sulfur atmosphere for 5–15 min to allow the formation of CZTS. Secondary phases such as Cu₂S, SnS, and Cu₂SnS₃ were found in the annealed samples when the annealing temperature was lower than 580 °C. They proposed that the secondary ZnS and Cu₂SnS₃ phases reacted to form CZTS when the annealing temperature was above 580 °C. Solar cells made from the CZTS samples prepared by sulfurization at 585 °C for 12 min showed efficiencies as high as 7.3%.

This is the highest efficiency reported to date for a pure CZTS-based solar cell prepared by electrodeposition.

This study involves the synthesis of CZTS-based solar cell prepared by electrodeposition method. This method is simple , inexpensive compared to other complicated vacuum based methods, allows fine control of the product composition, high throughput and very much cost effective for synthesis of quaternary chalcogenide thin film PV materials.

CHAPTER 3

THEORETICAL BACKGROUND

3.1 Interdiction

This chapter presents the general principles and theory of the various aspects of this research. It starts with a description of the physical and chemical properties of $\text{Cu}_2\text{SnZnS}_4$ thin film. The fundamental principles of electrochemical deposition and cyclic voltammetry are addressed. Furthermore, the basic concepts of the devices fabricated in this thesis, which include p–n junctions, are discussed. This is followed by a brief discussion of the basic principles of solar cell devices. In addition, this chapter addresses the principles underlying the operation of the fabrication and characterization equipment, as well as how to use theoretical equations to find the values of the parameters that describe the properties of the thin films and the performance of the devices.

3.2 Characteristics of $\text{Cu}_2\text{SnZnS}_4$ Thin Film

CZTS (copper zinc tin sulfide, with formula $\text{Cu}_2\text{SnZnS}_4$) solar cell research has been conducted extensively in recent years mainly because it is composed of elements that are not only inexpensive, but also non-toxic. CZTS is a p-type semiconductor, and is used as an absorber material in solar cells. In contrast, the elements used in the more common copper indium gallium selenide (CIGS) solar cells are both expensive and toxic. The reason CZTS cells are inexpensive is because the elements that comprise these cells are found abundantly in the earth's crust [60]. This allows the low-cost manufacture of solar cells in high volumes. While researchers have been able to

produce CIGS cells of high efficiency, the efficiency of CZTS cells is not comparable. However, in addition to being inexpensive and non-toxic, CZTS offers good optical and electronic properties. Thus, it is considered to be a promising semiconductor material for use in solar cells.

3.2.1 Structural Properties

Crystallographically, CZTS has two main structures, recognized as the kesterite type and stannite type structures. These two structures are alike except for the dissimilar arrangements of their 'Cu' and 'Zn' atoms (Figure 3.1). The structural differences are related to a different order in the cation sublattice: Kesterite, with space group $I4$, is characterized by alternating cation layers of CuSn, CuZn, CuSn, and CuZn at $z=0, 1/4, 1/2,$ and $3/4,$ respectively, whereas in the stannite structure, with $I4m$ symmetry, ZnS layers alternate with Cu_2 layers. Tin and sulfur ions occupy the same lattice positions in both structures. However, CZTS materials usually appear in kesterite phase because it is more thermodynamically stable than the stannite phase [60, 61]. However, the energy difference between the kesterite and stannite type structures is very small; only about 3 meV per atom, indicating that the stannite type structure may also be obtained under standard preparation conditions.

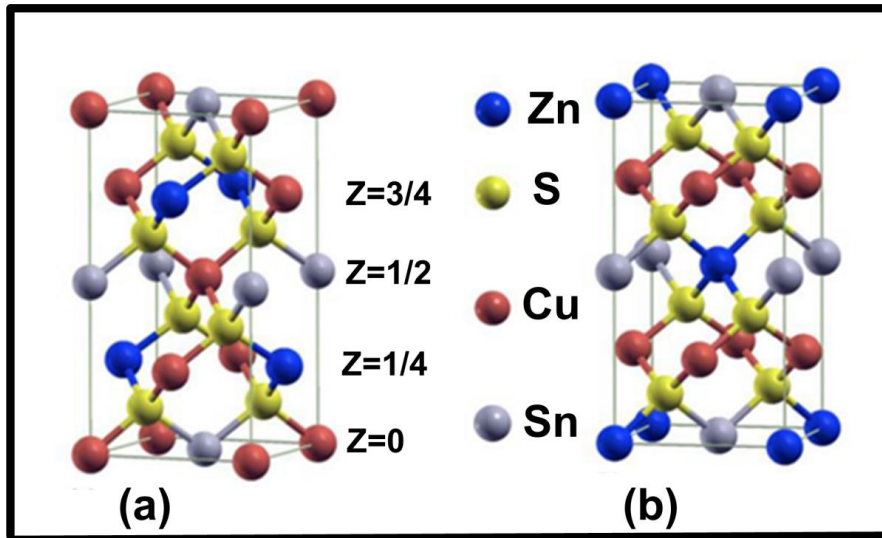


Figure 3.1 Schematic representations of the kesterite (a) and stannite (b) structures [62]

Kesterite materials (Kesterite is defined a sulfide mineral with a formula $\text{Cu}_2(\text{Zn,Fe})\text{SnS}_4$) belong to the family of chalcogenides. Some examples of this group include sphalerite (ZnS), chalcopyrite (e.g., CuInS_2), and kesterite (e.g., $\text{Cu}_2\text{ZnSnS}_4$) as shown in Figure 3.2 [30]. The option of replacing the rare and expensive indium with cheap and available Sn and Zn, while retaining main semiconductor properties such as nearly the same energy gap as that of the highly successful chalcopyrite absorber materials, makes CZTS attractive for large-scale photovoltaics manufacturing.